Journal of Nuclear Materials 390–391 (2009) 785–788

Contents lists available at ScienceDirect

Journal of Nuclear Materials

journal homepage: www.elsevier.com/locate/jnucmat

Plasma interactions with the outboard chamber wall in DIII-D

D.L. Rudakov [a,*], J.A. Boedo [a], J.H. Yu [a], N.H. Brooks [b], M.E. Fenstermacher [c], M. Groth [c], E.M. Hollmann [a], C.J. Lasnier [c], A.G. McLean [d], R.A. Moyer [a], P.C. Stangeby [d], G.R. Tynan [a], W.R. Wampler [e], J.G. Watkins [e], W.P. West [b], C.P.C. Wong [b], R.J. Bastasz [f], D. Buchenauer [f], J. Whaley [f]

[a] University of California-San Diego, 9500 Gilman Drive, Mail code 0417, La Jolla, CA 92093-0417, USA
[b] General Atomics, P.O. Box 85608, San Diego, CA 92186-5608, USA
[c] Lawrence Livermore National Laboratory, P.O. Box 808, Livermore, CA 94551, USA
[d] University of Toronto Institute for Aerospace Studies, Toronto, Canada M3H 5T6
[e] Sandia National Laboratories, P.O. Box 5800, Albuquerque, NM 87185, USA
[f] Sandia National Laboratories, P.O. Box 969, Livermore, CA 94551-0969, USA

ARTICLE INFO

PACS:
52.20
52.55
52.40.H

ABSTRACT

Erosion of the main chamber plasma-facing components is of concern for ITER. Plasma interaction with the outboard chamber wall is studied in DIII-D using Langmuir probes and optical diagnostics. Fast camera data shows that edge localized modes (ELMs) feature helical filamentary structures propagating towards the outboard wall. Upon reaching the wall, filaments result in regions of local intense plasma–material interaction (PMI) where peak incident particle and heat fluxes are up to two orders of magnitude higher than those between ELMs. In low density/collisionality H-mode discharges, PMI at the outboard wall is almost entirely due to ELMs. A moderate change of the gap between the separatrix and the outer wall strongly affects PMI intensity at the wall. Material samples exposed near the outboard wall showed net carbon deposition in high-density discharges (near the Greenwald limit) and tendency towards net erosion in lower density discharges (~0.45 of the Greenwald limit).

1. Introduction

Limiting plasma–material interactions (PMI) to acceptable levels presents one of the most difficult challenges for next-step fusion devices such as ITER [1]. The plasma facing components (PFCs) in ITER have to withstand incident fluxes of particles and energy at least an order of magnitude higher in size and duration than those encountered in present day tokamaks [1]. Though most of the energy and particles crossing the last closed flux surface (LCFS) into the scrape-off layer (SOL) are expected to be transported into the divertor where the PMI is strongest [2], plasma contact with main chamber components is non-negligible. Of particular concern are the impulsive loads due to transient events such as disruptions and edge-localized modes (ELMs). Studies at contemporary tokamaks have shown that ELMs can drive an appreciable portion of the total particle and energy exhaust far in the SOL and to the main chamber PFCs [3–22]. Moreover, it has been established that ELMs in the SOL have a filamentary structure [7,12–19,21,22], and individual filaments reaching the main chamber wall can cause localized intense PMI [3,8,10,12–19,21,22]. If this happens in ITER, it may cause enhanced erosion or even local melting of beryllium PFCs. We should note, however, that large ELMs capable of damaging the main wall structures would also put unacceptably high loads on the divertor plates, and should therefore be avoided. Nevertheless, adequate gaps between the wall and the separatrix should be maintained to avoid excessive erosion of the main wall PFCs.

2. Structure of the DIII-D outboard SOL and diagnostic arrangement

Fig. 1(a) shows a poloidal cross-section of a typical lower single-null (LSN) equilibrium in DIII-D showing the LCFS and a number of SOL magnetic flux surfaces. There are three distinct regions in the low field side (LFS) SOL [12,16]. (1) The "Divertor SOL" (DSOL) is the region where magnetic field lines connect from the outboard to the inboard side of the torus. (2) The "Limiter SOL" (LSOL) is the region where both ends of the magnetic field lines terminate on the divertor baffles (highlighted by thick lines in Fig. 1(a)). In configurations with a large upper gap (UG) and/or small outer wall gap (OWG) the LSOL may not exist. (3) Further radially outwards from the LSOL is the "Outer Wall Shadow" (OWS) region, where magnetic field lines terminate at the outer wall near the midplane. There are three bumper limiters (BLs) on the outer wall separated

* Corresponding author.
E-mail address: rudakov@fusion.gat.com (D.L. Rudakov).

0022-3115/$ - see front matter © 2009 Elsevier B.V. All rights reserved.
doi:10.1016/j.jnucmat.2009.01.208

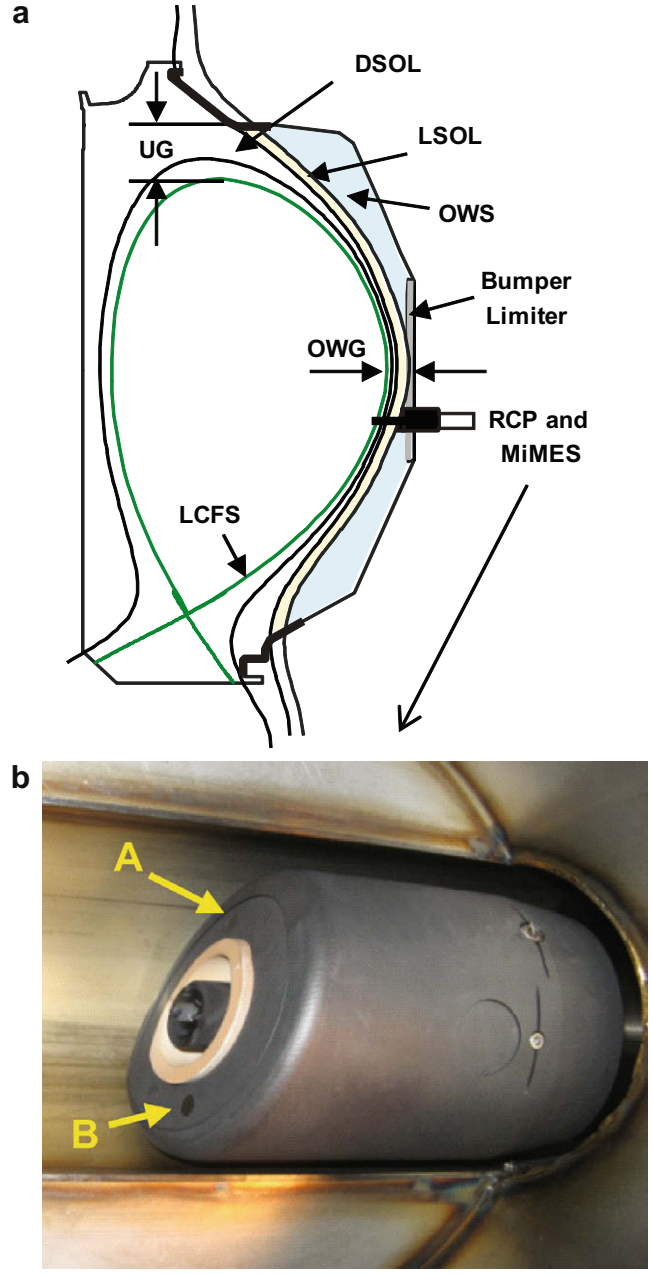

Fig. 1. (a) Diagnostic arrangement and structure of the DIII-D SOL in a LSN magnetic configuration; (b) RCP with MiMES inside the airlock chamber.

toroidally by approximately 120° and protruding ~2 cm inwards from the wall tile radius.

Previous studies of plasma interaction with the LFS chamber wall in DIII-D [12,16] relied almost exclusively on the mid-plane reciprocating probe array (RCP) and a fast profile reflectometer. A number of new diagnostics useful for wall PMI studies have recently been commissioned. A fast framing CMOS camera (Phantom 7.1) with a tangential view of the outboard chamber wall and spatial resolution of about 5 mm has been successfully used [22]. Two new filterscopes (telescopes with spectral line filters coupled to photomultipliers) have been installed, one with a view of a mid-plane portion of a bumper limiter and another with a view of the wall tiles nearby. In addition, the capability to install material samples at the outer shield of the RCP (Midplane Material Evaluation Station or MiMES) has been recently implemented. This allows *in-situ* measurements of net erosion/deposition near the LFS chamber wall. Samples can be exchanged through an airlock. A photograph of MiMES inside the airlock chamber is shown in Fig. 1(b). Locations of depth-marked graphite button samples used for net erosion/deposition measurements are marked by arrows.

3. Experimental results

Plasma interactions with the outboard wall were studied in LSN H-mode discharges with the following parameters: toroidal magnetic field, $B_T = 1.7–2.1$ T, plasma current, $I_p = 1–1.4$ MA, neutral beam heating power, $P_{NBI} = 1.5–7$ MW, line-average plasma density, $\bar{n}_e = 0.5–1.2 \times 10^{20} m^{-3}$, density normalized to Greenwald limit, $f_{GW} \equiv n_e/n_{GW} = 0.35–1$, pedestal collisionality, 0.5–12. The fraction of the pedestal energy lost per ELM, $\Delta W_{ELM}/W_{ped}$, decreases with the increasing density from 15% to 25% at $f_{GW} \sim 0.35$ to below 5% at $f_{GW} \sim 1$ [4], while the ELM frequency increases from tens to a few hundred of Hertz. Recently two series of reproducible LSN H-mode discharges dedicated to PMI studies in the divertor and main chamber were performed. The discharges had similar equilibrium shape and stored pedestal energy, but the first series of discharges were high-density, $f_{GW} \sim 0.9–1$, and the second series were of lower density $f_{GW} \sim 0.45$. The pedestal collisionality varied by more than a factor of 10, being 10–12 in the higher density series and 0.7–1.0 in the lower density case. The energy lost per ELM in the higher density discharges was 6–10 kJ at ELM frequency of 200–250 Hz, and in the lower density discharges, 30–45 kJ at ELM frequency of 50–70 Hz, so the overall power exhaust by ELMs was comparable between the two series.

Fast camera data shows that ELMs in the LFS edge and SOL feature helical filamentary structures aligned with the local magnetic field that propagate radially towards the wall [22]. The filament radial propagation velocity is estimated from the tangential view of the D_α (656 nm) emission (as a known distance between the tangency point and the wall divided by the propagation time measured from the camera data) to be 500 ± 400 m/s [22], and is consistent with the $E \times B$ velocity of ~700 m/s inferred from the probe data [14,16] and the ELM density pulse propagation velocity of ~500 m/s as estimated from reflectometer data [5]. Upon reaching the wall, the filaments cause PMI that is clearly observed in D_α emission by the fast camera and filterscopes due to release of neutrals from the wall tiles. Fig. 2 shows the D_α emission measured by the bumper limiter filterscope in the high ($f_{GW} \sim 1$, upper trace) and low ($f_{GW} \sim 0.45$, lower trace) density discharges. Peak signal during ELMs is a factor of 2.5–3 higher in the higher density case, while between ELMs it is higher by a factor of 20–30. Therefore, the relative contribution of ELMs is larger in the lower density case.

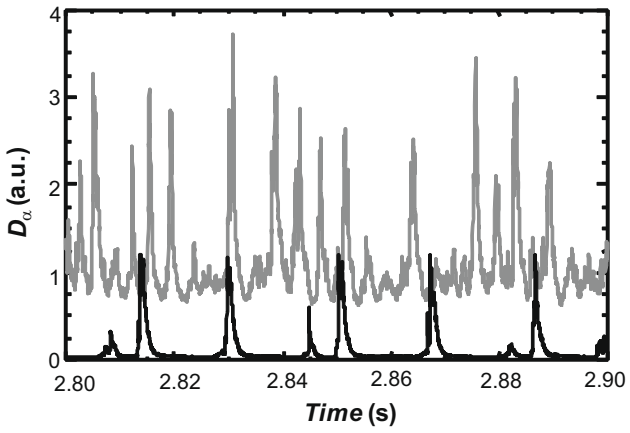

Fig. 2. D_α emission measured by the bumper limiter filterscope in a high ($f_{GW} \sim 1$, upper trace) and low ($f_{GW} \sim 0.45$, lower trace) density discharges.

The data of Fig. 2 are consistent with an earlier conclusion made from the probe data that the relative contribution of ELMs to the (parallel) particle flux arriving at the outboard wall decreases with increasing discharge density [16]. Fig. 3 shows the relative contribution of ELMs to the parallel particle (a) and heat (b) fluxes derived from RCP data measured a few millimeters inside of the OWS border. The particle flux is calculated as $\Gamma_{||} = j_{si}/e$ and the heat flux as $q_{||} = 7kT_e j_{si}/e$, where j_{si} is the ion saturation current density, T_e is the electron temperature, and e is the electron charge. Each point in Fig. 3 represents a ratio of the integral flux over ELMs to the total integral flux (over ELMs and inter-ELM periods) [16]. Points marked by solid circles are obtained from a moving probe data over individual ELMs (where inter-ELM fluxes are estimated as half-sum of fluxes just before and just after the ELM analyzed). Points marked by the open squares are from the above-mentioned discharges dedicated to PMI studies, obtained from stationary probe data averaged over 20–40 ELMs. There was no T_e measurement available in the higher density discharge series, so the heat flux data are missing. The relative contribution of ELMs to both fluxes tends to decrease with the density, though for the heat flux the trend is not so pronounced. ELM contribution to the net local heat flux is somewhat higher compared to the particle flux, which is not surprising, given that both density and temperature inside the ELM filaments are above the background values [12–18]. We should note that the expression we used to calculate the heat flux assumes that the ion temperature, T_i, within ELM filaments is equal to T_e, whereas it has been experimentally shown in JET that in ELM filaments T_i is higher than T_e by a factor of 2–3 [17]. Thus, relative contribution of ELMs to the wall heat flux may be even higher than shown in Fig. 3.

While propagating through the SOL, ELM filaments are depleted of particles and energy by parallel losses [18], and may partially or fully decay before reaching the wall. This is illustrated in Fig. 4 showing radial profile of the peak ion saturation current, I_{si}, within ELM filaments (squares) measured by the RCP in the far SOL of a high-density ($f_{GW} \sim 1$) discharge, one of the high-density series mentioned above. These discharges had a large upper gap (9.3 cm) and no LSOL. ELM frequency in the discharge shown was ~220 Hz, energy lost per ELM 6–10 kJ. Within a radial distance of ~4 cm the filament peak density decays by almost two orders of magnitude (the e-folding length is ~10 mm). Throughout the region shown it remains about 10× greater than the inter-ELM background (diamonds). Background density e-folding length is ~6 mm near the OWS boundary; the apparent flattening of the background profile closer to the wall is due to poor signal-to-noise ratio in this region. Later in the discharge, the outer wall gap was transiently reduced by 3 cm [Fig. 5(a)]. This resulted in increases in both filament amplitude and background density in the DSOL and throughout most of the OWS region [Fig. 4(b)]. E-folding lengths for both filament and background densities with the smaller gap were close to 10 mm. The BL and wall filterscopes evidenced increased PMI at the LFS wall manifesting itself by an increase in D_α emission [Fig. 5(b), BL filterscope signal from a similar discharge shown]. In subsequent discharges the wall gap was transiently increased by 3 cm resulting in ~4× reduction of the peak D_α emission during ELMs. Thus a moderate change of the OWG has a significant effect at the level of plasma interaction with the LFS wall. Work is in progress to compare ELM filament models [18] with the experimental results in Figs. 3 and 4 [23].

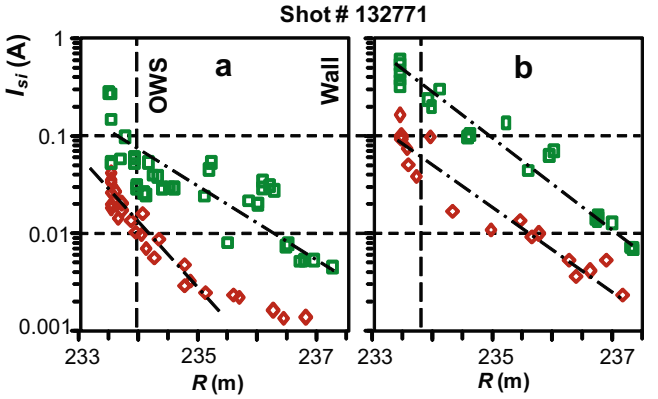

Fig. 4. Radial profiles of the peak I_{si} within ELM filaments (squares) and between-ELM background (diamonds) in the far SOL of a high density ($f_{GW} \sim 1$) LSN discharge with an outer wall gap of 9.3 cm (a) and 6.3 cm (b).

Exposures of graphite button samples installed on the plasma-facing side of MiMES [Fig. 1(b)] have been performed in both high and low density discharge series. During the high-density expo-

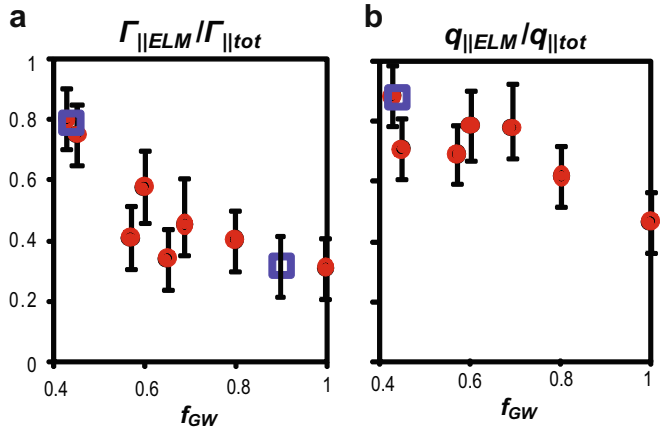

Fig. 3. Relative contribution of ELMs to the local parallel particle (a) and heat (b) fluxes just inside of the OWS boundary as a function of the normalized discharge density.

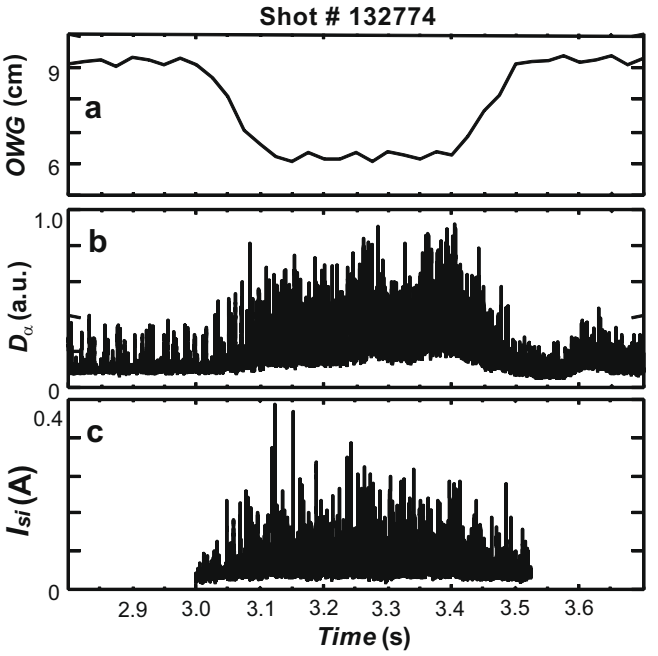

Fig. 5. Changes in LFS wall PMI with decreased outer wall gap (a). Shown are D_α emission measured by BL filterscope (b) and I_{si} to a probe fixed near the OWS boundary (c).

sure, the samples were in the OWS (~0.5 cm outside of the DSOL border) for a total of ~16 plasma-seconds and in the DSOL (~1.5 cm inside of OWS border) for ~12 plasma-seconds. The samples were implanted with a Si depth marker that allowed measurement of net erosion/deposition by ion beam analysis (IBA). The RCP was fixed during the exposure so that the tips measuring I_{si} were ~5 mm inwards of the sample location, as shown in Fig. 1(b). During OWG scans, I_{si} measured by the probe behaved similarly to D_α emission measured by BL and wall filterscopes [Fig. 5(c)].

The exposed button samples were analyzed by IBA at the Sandia National Laboratory. Net carbon deposition was measured on both samples exposed in the high-density discharge series, 24 nm on sample A and 40 nm on sample B (with the measurement uncertainty of ±10 nm). Judging by this result, in high density conditions with small ELMs, LFS main chamber PFCs are not subject to any significant erosion, and may even get net deposition. The exposure has been repeated in the lower density discharge series for a total of 10 discharges (~40 plasma seconds) with the samples located in DSOL, ~5 mm inside of OWS boundary. The measured change in the marker depth gave 13 nm of erosion on sample A and 10 nm of erosion on sample B. While being barely out of the uncertainty of the measurement, this result suggests that in lower density regimes with larger ELMs net erosion of the outboard main chamber PFCs is more likely to occur.

4. Summary and conclusion

Experimental evidence shows that there is an appreciable plasma interaction with the outboard main chamber wall in DIII-D. The relative contribution of ELMs to PMI with the LFS chamber wall decreases with increasing discharge density, which, in DIII-D, is coupled to increasing pedestal collisionality. Since ITER will have high normalized density and low collisionality, it is not clear how large the relative importance of ELMs for the main chamber PMI will be. Even at high density close to the Greenwald limit, ELM filaments may reach the LFS wall and cause erosion of the wall tiles. However, initial material studies in DIII-D using MiMES did not reveal any significant erosion, and even showed some net deposition in high-density conditions. A moderate increase of the gap between LCFS and the wall may decrease PMI intensity appreciably. Therefore, if plasma interaction with the main chamber wall is determined to be a challenge for ITER, provision for an increased wall gap may be advantageous.

Acknowledgment

This work was supported by the US Department of Energy under DE-FG02-07ER54917, DE-FC02-04ER54698, DE-AC52-07NA27344, and DE-AC04-94AL85000.

References

[1] G. Federici et al., Nucl. Fusion 41 (2001) 1967.
[2] P.C. Stangeby, The Plasma Boundary of Magnetic Fusion Devices, IOP Publishing, 2000.
[3] Ph. Ghendrih et al., J. Nucl. Mater. 313–316 (2003) 914.
[4] A.W. Leonard et al., Phys. Plasmas 10 (2003) 1765.
[5] M.E. Fenstermacher et al., Plasma Phys. Control. Fus. 45 (2003) 1597.
[6] B. Goncalves et al., Plasma Phys. Control. Fus. 45 (2003) 1627.
[7] A. Kirk et al., Phys. Rev. Lett. 92 (2004) 245002.
[8] A. Herrmann et al., Plasma Phys. Control. Fus. 46 (2004) 971.
[9] M. Endler et al., Plasma Phys. Control. Fus. 47 (2005) 219.
[10] A. Herrmann et al., J. Nucl. Mater. 337–339 (2005) 697.
[11] N. Asakura et al., J. Nucl. Mater. 337–339 (2005) 712.
[12] D.L. Rudakov et al., J. Nucl. Mater. 337–339 (2005) 717.
[13] J.A. Boedo et al., J. Nucl. Mater. 337–339 (2005) 771.
[14] J.A. Boedo et al., Phys. Plasmas 12 (2005) 072516.
[15] A. Kirk et al., Plasma Phys. Control. Fus. 47 (2005) 995.
[16] D.L. Rudakov et al., Nucl. Fusion 45 (2005) 1589.
[17] R.A. Pitts et al., Nucl. Fusion 46 (2006) 82.
[18] W. Fundamenski, R.A. Pitts, JET-EFDA contributors, Plasma Phys. Control. Fus. 48 (2006) 109.
[19] A. Kirk et al., Plasma Phys. Control. Fus. 48 (2006) B433.
[20] A.W. Leonard et al., J. Nucl. Mater. 363–365 (2007) 1066.
[21] B. Lipschultz et al., Nucl. Fusion 47 (2007) 1189.
[22] J.H. Yu et al., Phys. Plasmas 15 (2008) 032504.
[23] P.C. Stangeby, private communication.